CRYSTAL GROWTH & DESIGN

pubs.acs.org/crystal

Communication

Crystal Structures of Lignocellulosic Furfuryl Biobased Polydiacetylenes with Hydrogen-Bond Networks: Influencing the Direction of Solid-State Polymerization through Modification of the Spacer Length

Pierre Baillargeon,* Raphaël Robidas, Olivier Toulgoat, Zacharie Michaud, Claude Y. Legault, and Tarik Rahem

Cite This: *Cryst. Growth Des.* 2022, 22, 2812−2823

Read Online

ACCESS | Metrics & More | Article Recommendations | Supporting Information

ABSTRACT: We present the topochemical polymerization of two lignocellulosic biobased diacetylenes (DAs) that only differ by an alkyl spacer length of 1 methylene (n = 1) or 3 methylene units (n = 3) between the diyne and carbamate functionalities. Their crystalline molecular organizations have the distinctive feature of being suitable for polymerization in two potential directions, either parallel or skewed to the hydrogen-bonded (HB) network. However, single-crystal structures of the final polydiacetylenes (PDAs) demonstrate that the resulting orientation of the conjugated backbones is different for these two derivatives, which lead to HB supramolecular polymer networks (2D nanosheets) for n = 1 and to independent linear PDA chains with intramolecular HBs for n = 3. Thus, spacer length modification can be considered a new strategy to influence the molecular orientation of conjugated polymer chains, which is crucial for developing the next generation of materials with optimal mechanical and optoelectronic properties. Calculations were performed on model oligodiacetylenes to evaluate the cooperativity effect of HBs in the different crystalline supramolecular packing motifs and the energy profile related to the torsion of the conjugated backbone of a PDA chain (i.e., its ability to adopt planar or helical conformations).

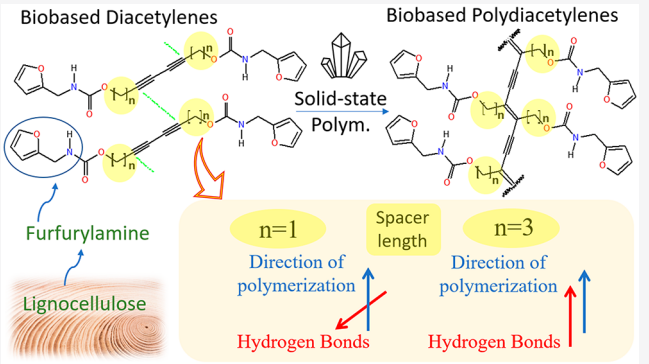

Polydiacetylenes (PDAs) are a class of semiconductor polymers that have attracted the attention of the scientific community due to their unique optoelectronic properties, in particular, their blue-red colorimetric transition when the leading conjugated backbone chains are disturbed by various external stimuli.[1,2] This feature has been exploited in a wide range of sensing applications,[3−5] going from virus detection,[6] to dosimeter system,[7] and so on.[8,9] The synthesis of PDA has been achieved in several forms, such as liposomes (also referred to as vesicles),[10−12] micelles,[13−15] Langmuir−Blodgett films,[16,17] strips,[18] nanotubes,[19,20] gels,[21,22] nanofibers,[23,24] and crystals.[25−29] In addition to applied research on this type of polymeric material, a fundamental understanding of the structure−property relationship of PDA can be obtained from crystallographic studies. Crystalline topochemical polymerization has been reported as an effective tool that offers control over polymers' molecular and supramolecular structures.[30−32] A recent review has described several other advantages of topochemical polymerization in the crystalline state over conventional solution-phase polymerization.[33] On the other hand, suitable packing requirements for monomers must be satisfied to achieve the solid-state polymerization of diacetylenes[34,35] (Figure 1a): (1) The C1−C4′ contact distance (r) on adjacent diacetylene moieties must be less than or equal to 4 Å, (2) the stacking translational distance (d) of the monomers must be close to 4.9 Å, and (3) the orientation angle (θ) between the DA rod and the stacking axis must be close to 45°.

However, these conditions are necessary but insufficient for the reaction to occur efficiently. Indeed, some examples in the literature suggest that if the hydrogen bond (HB) network is too close to the reactive DA, the topochemical reaction is partially inhibited and produces red PDA instead of the expected blue PDA with a long effective conjugation length.[36−38] This is probably one of the main reasons that flexible alkyl spacers with three or more methylenes between the DA reactive site and the

Received: March 10, 2022
Revised: April 5, 2022
Published: April 12, 2022

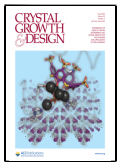

ACS Publications

© 2022 The Authors. Published by American Chemical Society

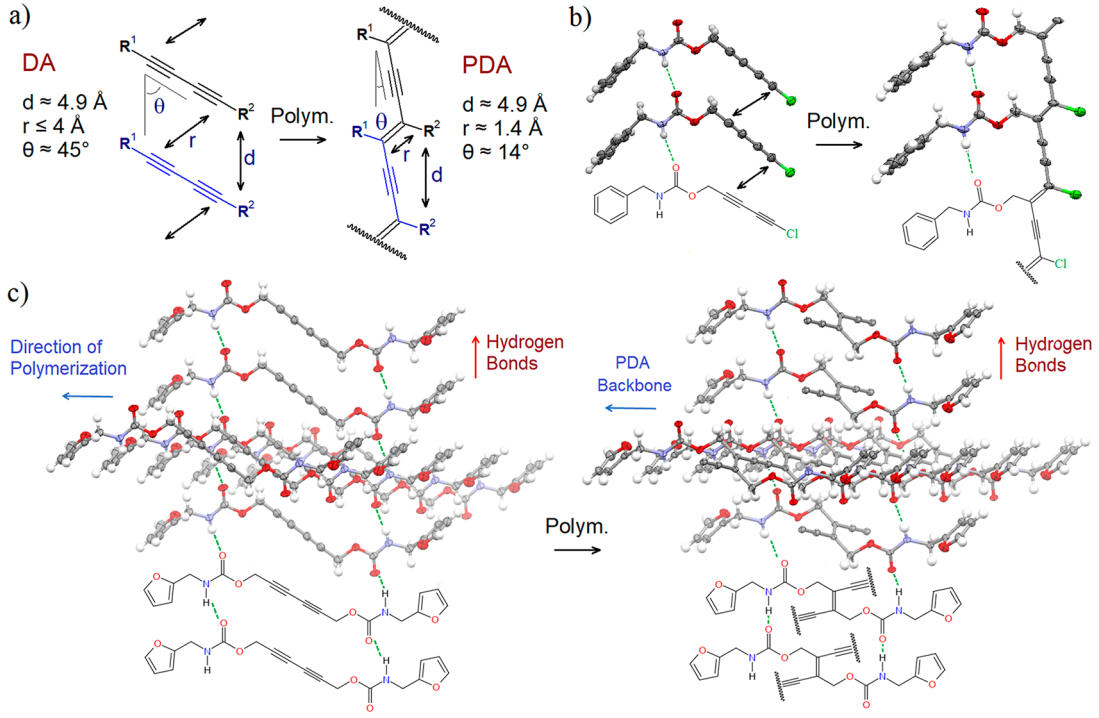

Figure 1. (a) Ideal geometrical conditions for the solid-state polymerization from DA to PDA. (b) Our previous work[27] on polychlorodiacetylene (PClDA) presenting a HB network close and parallel to the conjugated PDA backbone. (c) Our previous work[26] on biobased polydiacetylene having a HB network close but skewed to the conjugated PDA backbone.

group involved in the HB network have been widely used in PDA systems.[39−42] Our group focused on two exceptions that allowed us to determine the crystal structures of the resulting polymers even though HB networks were close to the DA functionalities:

- The first exception has been using a highly reactive chlorodiacetylene (Figure 1b).[27] Using urethane (carbamate) functionality, we successfully obtained a single crystal structure determination of a polychlorodiacetylene with an HB network close and parallel to the conjugated PDA backbone. To the best of our knowledge, it is the first example of a complete structural determination of this kind of compact and parallel HB arrangement in PDA. Moreover, interactions through C−Cl···π halogen bonds (XB) are present, and this is another example of the incorporation of XBs into polymer science. This field has gained increasing importance recently.[27,43−48]
- The second exception, also using the directional urethane functionality, consisted in the polymerization of DA in the direction skewed (forming an angle of 70°) to the HB network. This arrangement was first observed by the group of Collet in 1988.[49] However, there were no further investigations of this interesting molecular organization until our work with lignocellulosic biobased PDA in 2019 (Figure 1c).[26]

There have been numerous efforts to develop biobased polymers as a potential solution to reduce dependence on fossil resources.[50] In the case of PDA, we are the first group to report a furan-biobased PDA material.[26] Since furfural (**FUR**) has been identified as one of the most promising chemical platforms directly derived from biomass[51] and since furfurylamine (**FAM**) may either be obtained by reductive amination of furfural[52] or directly from biomass via a novel chemoenzymatic one-pot process,[53] our approach has focused on furfurylamine biobased diacetylene (**FAM-DA**) monomers as an interesting starting point in the development of environmentally friendly PDA materials (Figure 2a). More recently, Kim's group developed furfuryl alcohol biobased diacetylene (**FA-DA**) and the corresponding PDA. They exploited the furan heterocycle in Diels−Alder and retro Diels−Alder reactions, proving that furan-based DA and PDA constitute a promising new family of functional materials.[54] We herein investigated the effect of the spacer length (n = 1 or 3) on the direction of polymerization of **FAM-DAs** (Figure 2b). We present the synthesis of the new **FAM-DA-3CH2** derivative with a spacer of three methylenes (n = 3) and the comparative study between the single crystal topochemical polymerization of this new DA and our previous reported similar parent DA with a spacer of 1 methylene (n = 1).[26] Finally, based on atomic coordinates extracted from the X-ray single-crystal structures obtained from **FAM-PDA-1CH2** and **FAM-PDA-3CH2**, we evaluated the cooperative behaviors of the HB networks through DFT calculations (Figure 2c). Using semiempirical tight-binding calculations, we also assessed the torsional energy profile around the planar conformation of individual PDA chains with intramolecular HBs (Figure 2d).

SYNTHESIS

We synthesized derivative **FAM-DA-3CH2** in two steps (Scheme 1). At first, alkyne **1** was obtained from furfuryl isocyanate, which is commercially available or otherwise readily accessible from furfurylamine.[55] Second, using the Hay catalyst, we achieved the homocoupling reaction of the terminal alkyne **1** in 2 h 30 min to give the desired diacetylene.

RECRYSTALLIZATION

The test tubes containing the desired product (spotted by TLC analysis) were left at room temperature for 1 week with

https://doi.org/10.1021/acs.cgd.2c00307
Cryst. Growth Des. 2022, 22, 2812−2823

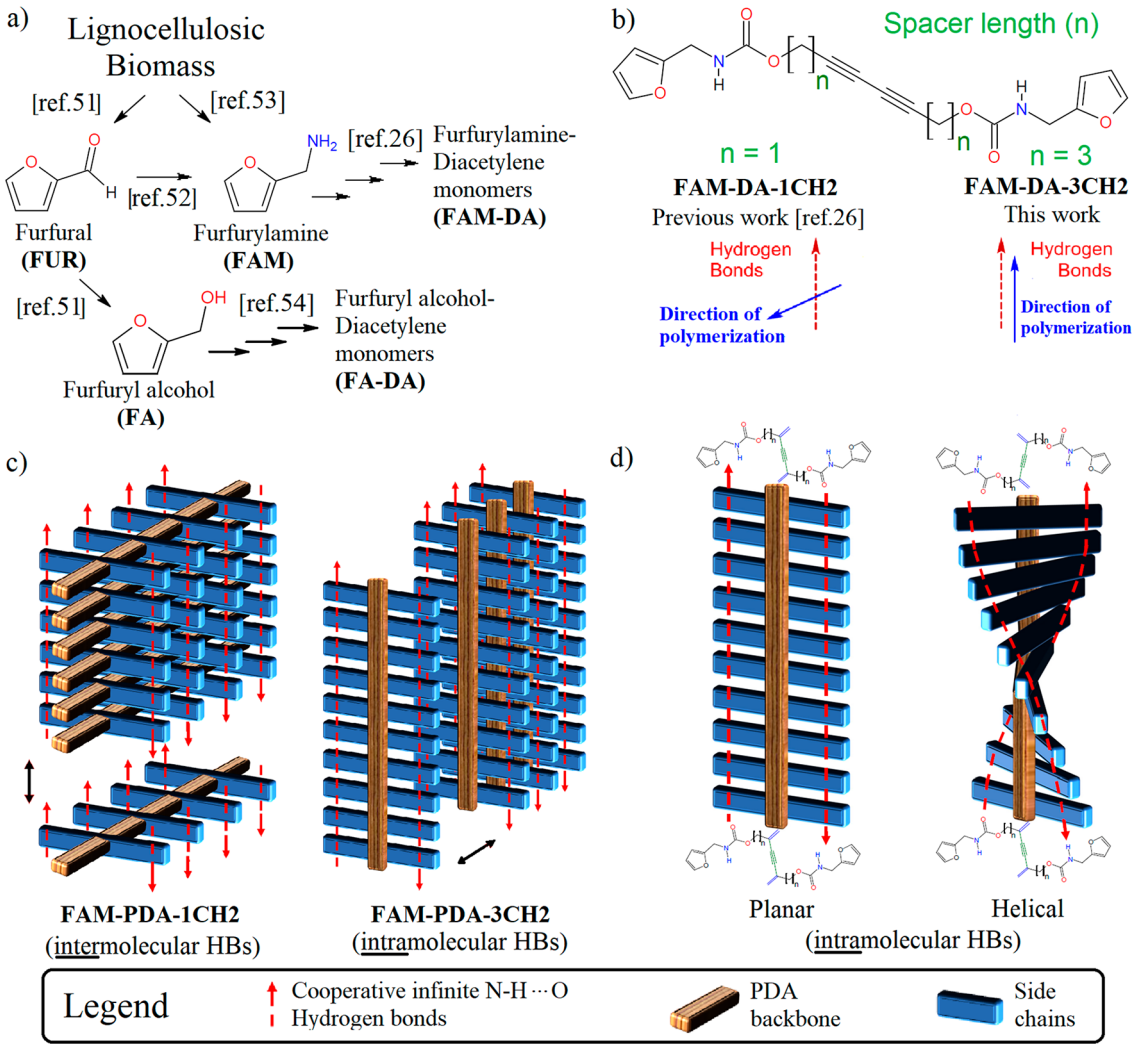

Figure 2. (a) Synthetic route from lignocellulosic biomass to furfurylamine (**FAM**)[51−53] and furfuryl alcohol (**FA**) to the corresponding furfurylamine-diacetylene (**FAM-DA**)[26] and furfuryl alcohol-diacetylene (**FA-DA**)[54] monomers. (b) Structures and direction of polymerization of the two studied diacetylenes which differ by an alkyl spacer length (n) of one methylene (n = 1) or 3 methylene units (n = 3) between the diyne and carbamate functionalities. (c) Schematic representation of HBs in the supramolecular motifs observed in the crystal structure of **FAM-PDA-1CH2** and **FAM-PDA-3CH2**. (d) Illustration of the conformational change between the planar and helical PDA backbone having intramolecular HBs.

Scheme 1. Synthetic Route of FAM-DA-3CH2

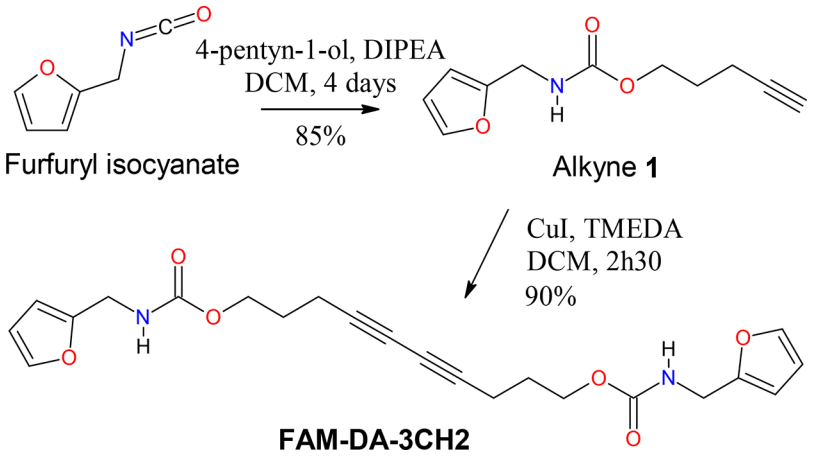

minimum light exposure following the flash chromatography purification procedure. The slow evaporation of the eluent of the chromatography directly resulted in the formation of colorless crystals with blue parts (Figure S1a), which suggests some degree of polymerization. Addition of dichloromethane (DCM) to these crystals in test tubes formed partially insoluble blue

https://doi.org/10.1021/acs.cgd.2c00307
Cryst. Growth Des. 2022, 22, 2812−2823

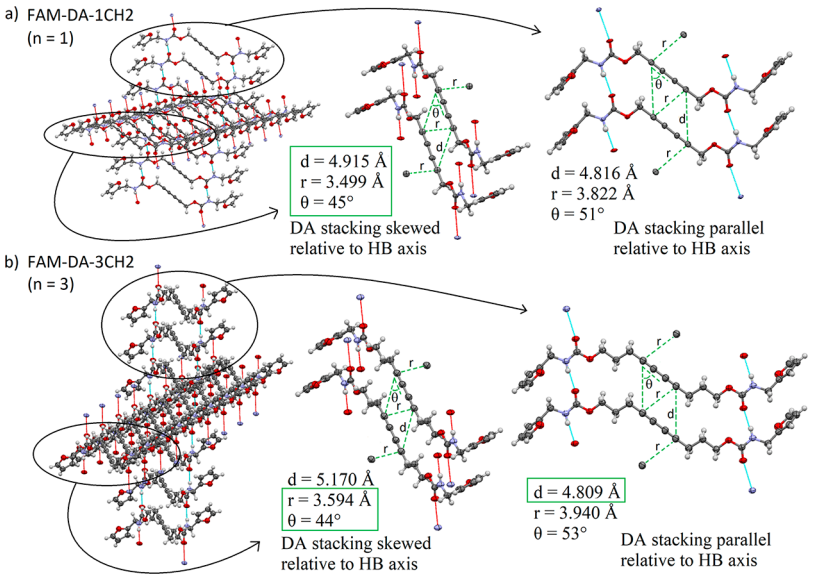

Figure 3. Geometrical parameters of the two potential directions of polymerization in DA single crystals of (a) **FAM-DA-1CH2** and (b) **FAM-DA-3CH2**. A green box was used to highlight the parameters whose values are closest to the optimal values. Displacement ellipsoids are drawn at the 40% probability level.

Figure 4. Picture of the crystal chunks of **FAM-DA-3CH2** used to study the color change after UV irradiation for (a) 0 min, (b) 5 min (picture shows the side not exposed to UV light), and (c) 20 min.

fibers (Figure S1b, 0.6 mg of insoluble material over a total of 18 mg); the major part of the sample remained in the form of the monomer **FAM-DA-3CH2** (97% if we consider the mass that could be dissolved and recovered with DCM). RAMAN spectroscopy also confirms that there are remaining monomers since the typical diacetylene peak at 2260.6 cm^{-1} is still present (Figure S7). Indeed, a plate-like specimen (Figure S1c) of **FAM-DA-3CH2** was used for the X-ray crystallographic analysis and revealed the structure of the desired monomer.

X-RAY SINGLE CRYSTAL STRUCTURE ANALYSIS OF THE DA

The crystal structure of **FAM-DA-3CH2** has an interesting feature similar to the parent crystal structure of **FAM-DA-1CH2**: the DA monomers stack in such a way that the polymerization may occur in two directions (Figure 3). Indeed, the geometrical requirements (Figure 1a) are respected for the topochemical polymerization of DA in both the direction parallel and the direction skewed to the HBs. The main difference comes from the fact that in the case of **FAM-DA-1CH2** (Figure 3a), all the parameters (d, r, and θ) have their values closest to the ideal conditions in the case of the polymerization skewed to the HBs. Unsurprisingly, polymerization proceeded in this direction.[26] In contrast, for **FAM-DA-3CH2** (Figure 3b), the parameters r and θ seem to favor the polymerization in the direction skewed to HB, while the parameter d seems to favor the reaction that occurs in the direction parallel to HB. To the best of our knowledge, this is the first example of a DA system in which such a competition is present and raises the following questions: What will be the favored direction? Which distance parameter (r or d) is more critical for the process? A more in-depth examination of the origin of the reported optimal distances r and d allowed us to provide potential answers to these questions. First, the optimal value of r has often referred to a distance less than or equal to the van der Waals (vdW) contact distance between the two reactive unsaturated carbon atoms. Thus, various values have been reported in the literature (3.4 Å,[56] 3.5 Å,[57,58] or 3.8 $Å^2$), since different methods can be used to determine the vdW distance.[59] Nevertheless, we did not find a clear explanation for the use of the vdW contact limit since the original r value reported by Enkelmann in 1984 was $r \leq 4$ Å based on diacetylene reactivity and crystallographic data.[34] Second, since the average distance between equivalent atoms along the final PDA backbone is about 4.9 Å, the intermolecular spacing d between DA must be as near as possible to this value. An experience reported by the Laugher group has shown that it should not deviate more than about 0.2 Å from the ideal value of 4.9 Å.[35] So, the range for the d value often reported in the literature (d = 4.7 to 5.2 Å)[60−62] seems inconsistent with a logical ±0.2 Å deviation (it should be reported as d = 4.7 to 5.1 Å). Moreover, the Laugher group suggests that the repeat distance d is the most critical of the two distances. Therefore, taking into account that the r distance is less critical, the parallel direction of polymerization should be favored with **FAM-DA-3CH2** (Figure 3b), since in the skewed direction, the d value (5.170 Å) is found to be outside the values recommended by Laugher (d = 4.7 to 5.1 Å) for topochemical reactivity (although it is within, but at the limit of, the traditional

https://doi.org/10.1021/acs.cgd.2c00307
Cryst. Growth Des. 2022, 22, 2812−2823

values reported in several articles of the literature (d = 4.7 to 5.2 Å)).

SINGLE CRYSTAL TOPOCHEMICAL POLYMERIZATION

If a **FAM-DA-3CH2** single crystal is heated at 60 °C for 6 days, the quality of X-ray diffraction (XRD) data is greatly diminished, but this is still sufficient to demonstrate that the resulting unit cell matches that of the initial monomer, even if the single crystal becomes darker (see Figure S2). Higher temperatures or longer heating times result in the loss of most of the diffraction of the single crystal, making structural analysis by XRD impossible under these conditions. We, therefore, opted for UV irradiation to solve this problem. Blue crystals (Figure 4a) of **FAM-DA-3CH2** have been irradiated for five (5) minutes at 254 nm. After this period, a golden metallic luster is observed on the crystals.

Nevertheless, some blue stains are still present on the side not exposed to UV (Figure 4b), which means that the process was done mainly on the surface and not in bulk. Fifteen (15) additional minutes of irradiation gave the crystals an almost completely golden color (Figure 4c). In Raman spectroscopy, the diacetylene peak of the monomer (2260.6 cm^{-1}, Figure S7) completely vanished, while typical bands of polydiacetylene at 1454.5 and 2073.5 cm^{-1} became the strongest signals of the spectrum (Figure S8).

Table 1. Determination of Polymer Concentration by the Residual Monomer Dissolution Method as a Function of UV Exposure Time of Crystalline Samples of FAM-DA-1CH2 and FAM-DA-3CH2

		FAM-DA-1CH2		FAM-DA-3CH2	
Entry	Exposure Time (min)	A (%) of soluble organic mass recovered	% polym.	B (%) of soluble organic mass recovered	% polym.
1	0	92	**8**	97	**3**
2	5	68	**32**	78	**22**
3	20	67	**33**	62	**38**
4	60	41	**59**	42	**58**
5	240	17	**83**	37	**63**

After a total of 1 h of irradiation, the conversion toward polymerization was estimated to be 58% based on the soluble mass of the monomer that was dissolved and recovered (Table 1, entry 4). The applicability of this gravimetric technique is relatively easy and general, but the accuracy in the measurements constitutes a significant drawback.[63] Also, depending on the size of the crystals, the penetration of UV rays to the bulk can vary. Nevertheless, we can follow approximately the progression of the polymerization. After 4 h of irradiation, the polymerization proportion reaches 63% (Table 1, entry 5). To confirm the determination of the crystallographic structure of polydiacetylene, we irradiated a small selected single crystal of **FAM-DA-3CH2** for 4 h before analyzing it successfully by X-ray diffraction. We can assume that irradiation is an efficient method for thin crystals like this one, as the bulk is not very far from the surface.

X-RAY SINGLE-CRYSTAL STRUCTURES ANALYSIS OF THE RESULTING FAM-PDA-3CH2

As discussed earlier, probably due to parameter d, the direction of chain propagation during the polymerization of **FAM-DA-3CH2** is parallel to the HB network, as seen in the resulting crystal structure **FAM-PDA-3CH2** (Figure 5a). As commonly observed during the polymerization of DAs, the unit-cell volume of the monomeric crystal is reduced (from 1034.6 $Å^3$ for **FAM-DA-3CH2** to 987.9 $Å^3$ for **FAM-PDA-3CH2**, ca. 5% contraction), and consequently the density is increased (from 1.324 g/cm^3 for **FAM-DA-3CH2** to 1.386 g/cm^3 for **FAM-**

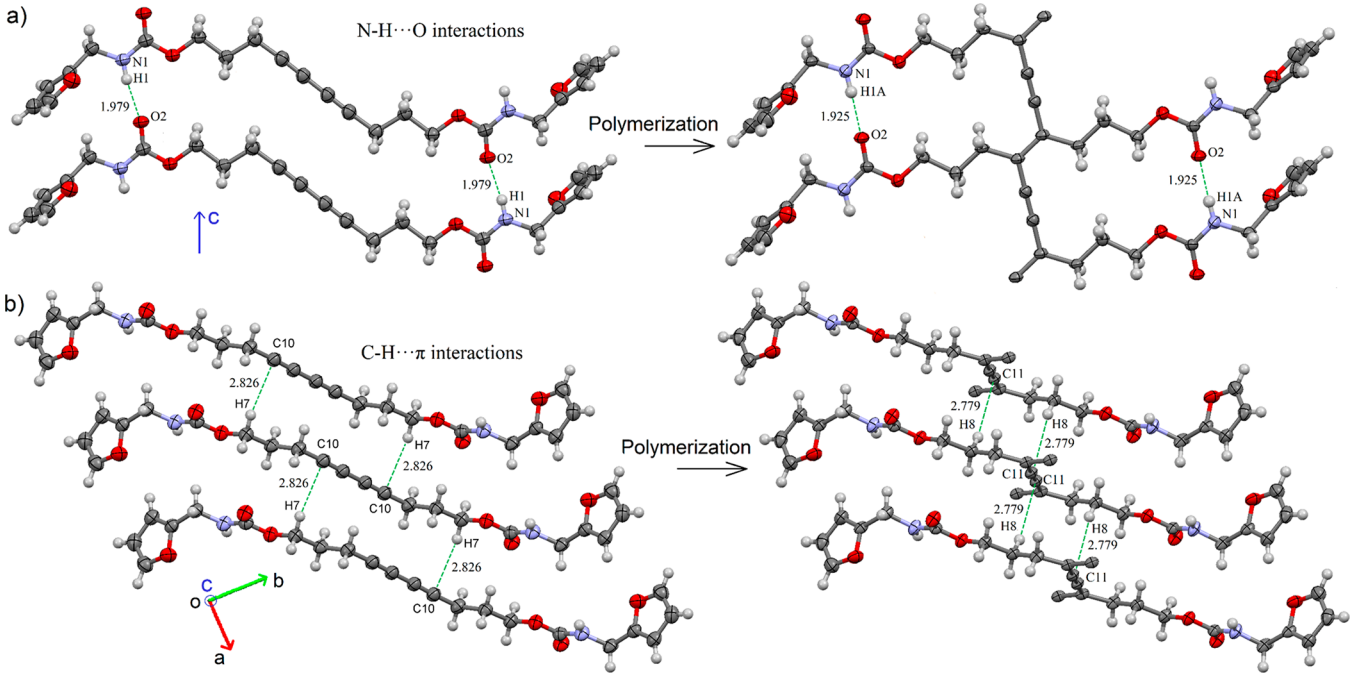

Figure 5. (a) Main directional intermolecular interactions (N—H···O hydrogen bonds) of the carbamate group observed in the crystal structure of **FAM-DA-3CH2** and the corresponding intramolecular HB interactions in **FAM-PDA-3CH2**. (b) Positional difference of the main C—H···π interactions present in **FAM-DA-3CH2** and **FAM-PDA-3CH2**. Displacement ellipsoids are drawn at the 40% probability level.

https://doi.org/10.1021/acs.cgd.2c00307
Cryst. Growth Des. 2022, 22, 2812−2823

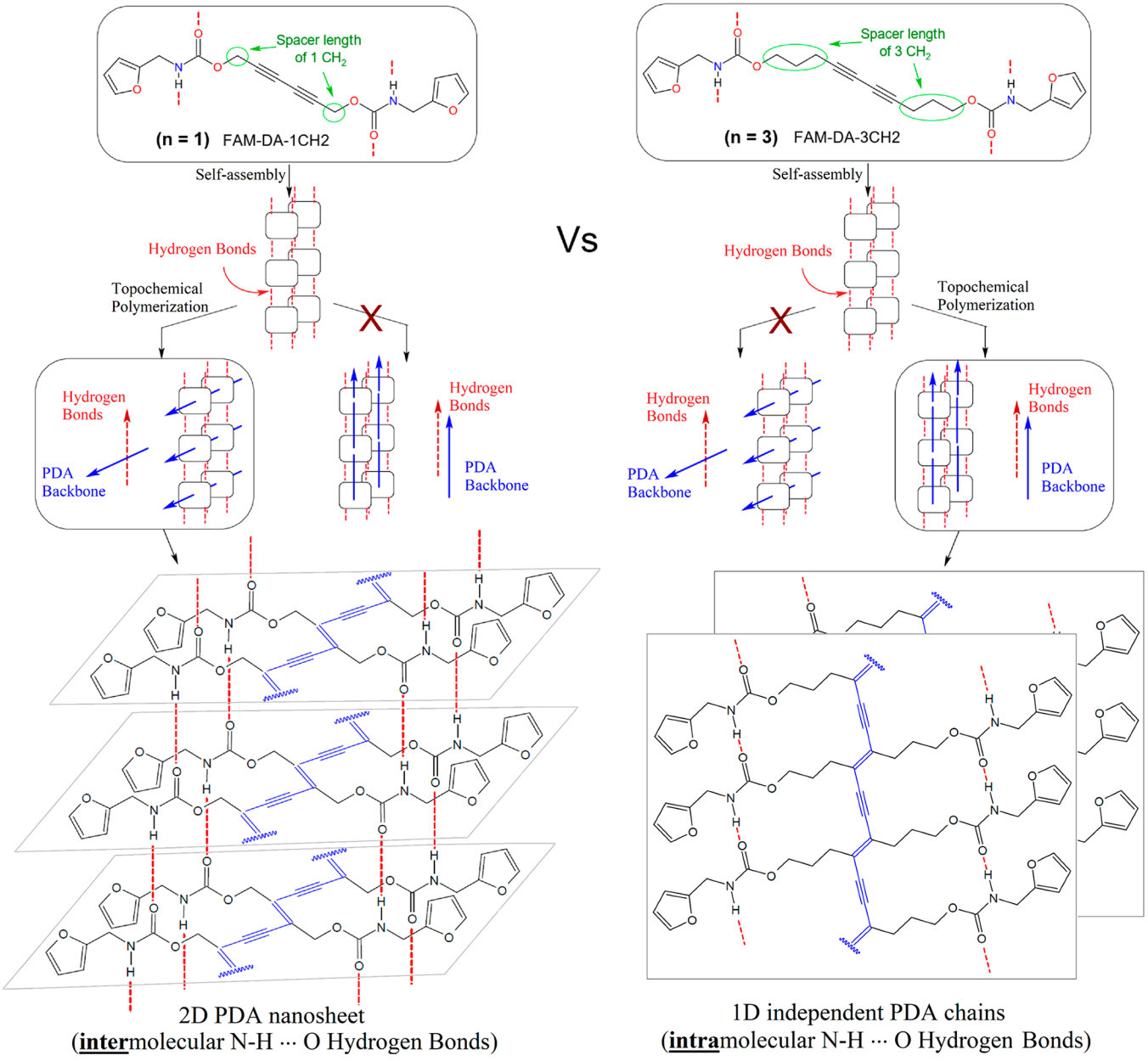

Figure 6. Illustration of the impact of the bond length modification on the direction of the polymerization of the furfurylamine biobased diacetylenes (**FAM-DAs**) and representation of the resulting HB network supramolecular architecture (left: 2D nanosheet for **FAM-PDA-1CH2**; right: 1D independent PDA chains for **FAM-PDA-3CH2**).

PDA-3CH2). The N−H···O HBs along the *c* axis shorten from 1.979 Å in the initial DA stack to 1.925 Å in the final polymer (Figure 5a). Meanwhile, along the *ab* plane, the C−H···π weak interactions between neighboring linear 1D supramolecular stacks of DA have shifted from the H7···C10 contact (2.826 Å, O−C**H**2···**C10**) in the initial monomer to a new H8···C11 contact (2.779 Å, O−CH2−C**H**2···**C11**) in the resulting polymer (Figure 5b).

■ COOPERATIVE HBS IN POLYMERS

Due to the different directions of polymerization of the initial DA monomers with various spacer lengths, the resulting supramolecular motifs observed in the crystalline state are very different for **FAM-PDA-3CH2** than those observed for **FAM-PDA-1CH2** (Figure 6). The main difference comes from the presence of an intermolecular N−H···O HB network between the PDA chains for **FAM-PDA-1CH2**, whereas with **FAM-PDA-3CH2**, we find rather intramolecular HBs. Since HBs may have a considerable impact on the final properties of the overall polymeric material[64−71] or on individual macromolecules,[72] we were interested in modeling simplified oligodiacetylenes (ODAs) to get information on the cooperative effects of the HBs. Indeed, cooperative HBs play a crucial role in shaping macromolecular conformations and governing macroscopic properties of biomacromolecules and synthetic polymers.[72,73] For example, cooperative interchain HB network links polypeptide chains together to form a two-dimensional (2D) rigid β-sheet motif,[74−76] and on the other hand, the cooperative intramolecular HBs may stabilize the helical conformation of a polypeptide chain (such as an α-helix). Thus, using a computational approach, we were interested in

https://doi.org/10.1021/acs.cgd.2c00307
Cryst. Growth Des. 2022, 22, 2812−2823

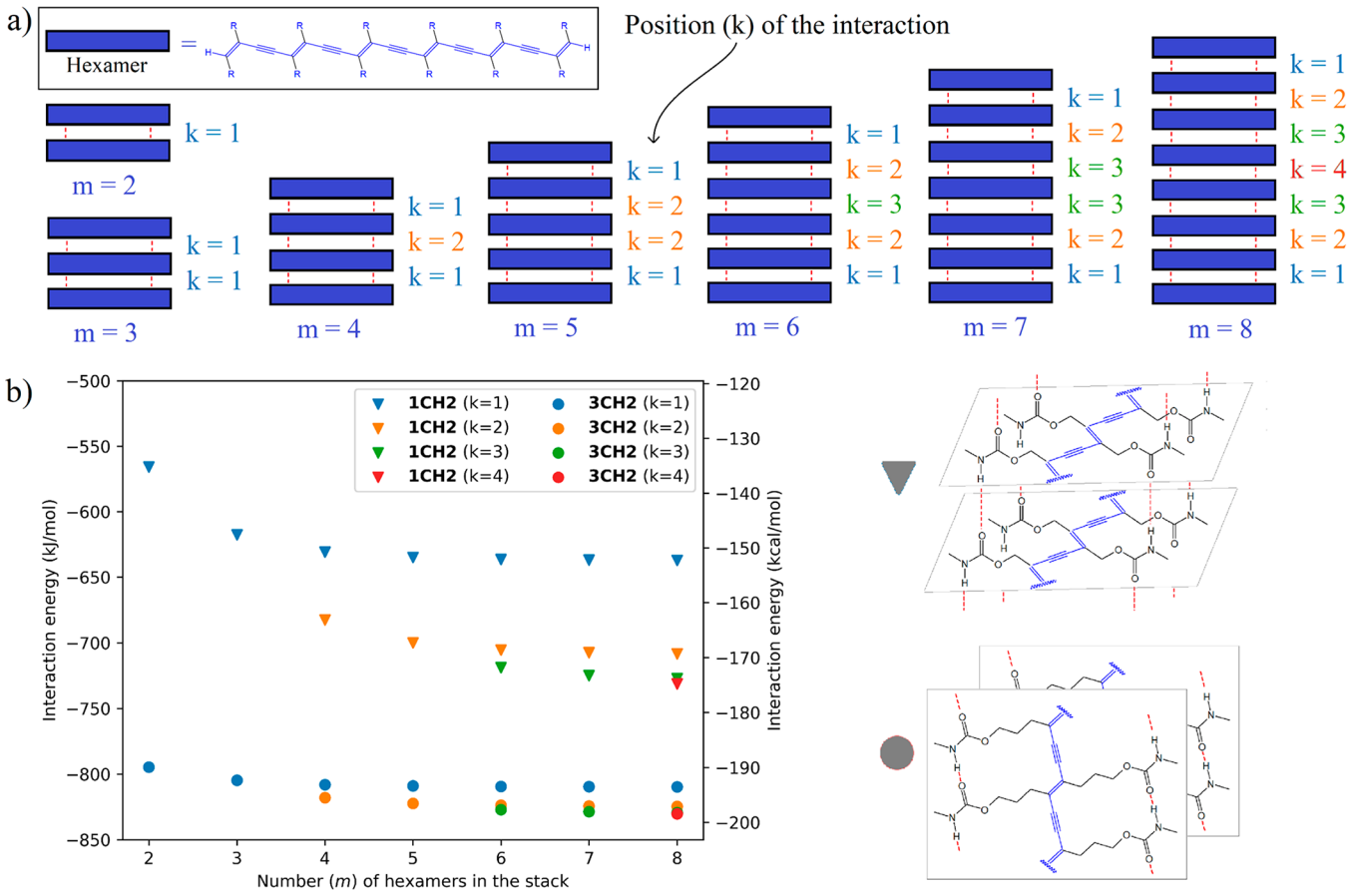

Figure 7. Interaction energies (B97D3/Def2SVP/W06) between the organized hexamer chains as a function of the number (m) of model hexamers forming the stack and as a function of the position (k) of the interaction in the stack. Note that hexamers without the furan cycles were used as model oligomers for the calculations.

- Studying the intermolecular cooperative effect of HBs in the 2D nanosheet of **FAM-PDA-1CH2**.
- Evaluating the potential well around the planar conformation of the PDA with intramolecular cooperative HBs.

COMPUTATIONAL STUDIES (COOPERATIVE HB EFFECT IN 2D NANOSHEETS)

We first compared the stabilization energy of the two types of 2D architectures, namely, 2D nanosheets built from PDA chains interlocked by N−H···O HBs in the case of **FAM-PDA-1CH2** or by C−H···π weak interaction in the case of **FAM-PDA-3CH2**. To do so, we extracted 2D supramolecular stacks of 2 to 8 hexamer structures from the X-ray single-crystal data (Figure 7a). In order to reduce the size of the systems and keep them computationally tractable, we removed the furan cycles on the PDA side chains. We then performed DFT single-point calculations (B97D3/Def2SVP with density fitting using W06 as basis set) on these model systems and calculated the interaction energies depending on the number (m) of molecules and the position (k) of the desired interaction in the stack (Figure 7b), using a similar approach to the one reported by Dannenberg.[77]

The first difference in behavior between the two studied PDA systems is highlighted by the variation of the interaction energies as the number of hexamer chains m in the stack increases. In the case of **FAM-PDA-1CH2**, where we have intermolecular hydrogen bonds, we go from an intermolecular interaction of −135.2 kcal/mol between two hexamers (m = 2, k = 1) to interaction energies ranging from −152.3 kcal/mol (k = 1) to −174.8 kcal/mol (k = 4) between two hexamers in a stacking of eight (m = 8) hexamers. This is evidence of a cooperativity effect that makes the HBs stronger as more units are added, in this case, up to 29% (39.6 kcal/mol) stronger in terms of interaction energy. By comparison, the **FAM-PDA-3CH2** present an interaction energy of −189.9 kcal/mol (m = 2, k = 1) to an interaction energy ranging from −193.5 kcal/mol (k = 1) to −198.4 kcal/mol (k = 4), an increase of interaction energy of only 4% (8.5 kcal/mol). This small cooperative effect can potentially come from C−H···π interaction, since it has already been reported in the literature to be involved in a cooperativity effect.[78] Nevertheless, we saw that the stack with intermolecular N−H···O interactions (**FAM-PDA-1CH2**) has a higher cooperativity effect (29% vs 4%) than the one without these interactions (**FAM-PDA-3CH2**).

Another known characteristic of the HB network's cooperativity is that the highest interaction value is located at the central position of the chain (for example, position k = 4 has higher energy interaction than position k = 1). We can extrapolate the curves using the equations proposed by Dannenberg,[77] resulting in maximal interaction energy of −176.2 kcal/mol at large m and k values in the **FAM-PDA-1CH2** model. Thus, our model's central interactions (k = 4) with eight hexamers have over 99% of the expected maximal interaction energy. Even the central interaction (k = 3) in the

https://doi.org/10.1021/acs.cgd.2c00307
Cryst. Growth Des. 2022, 22, 2812−2823

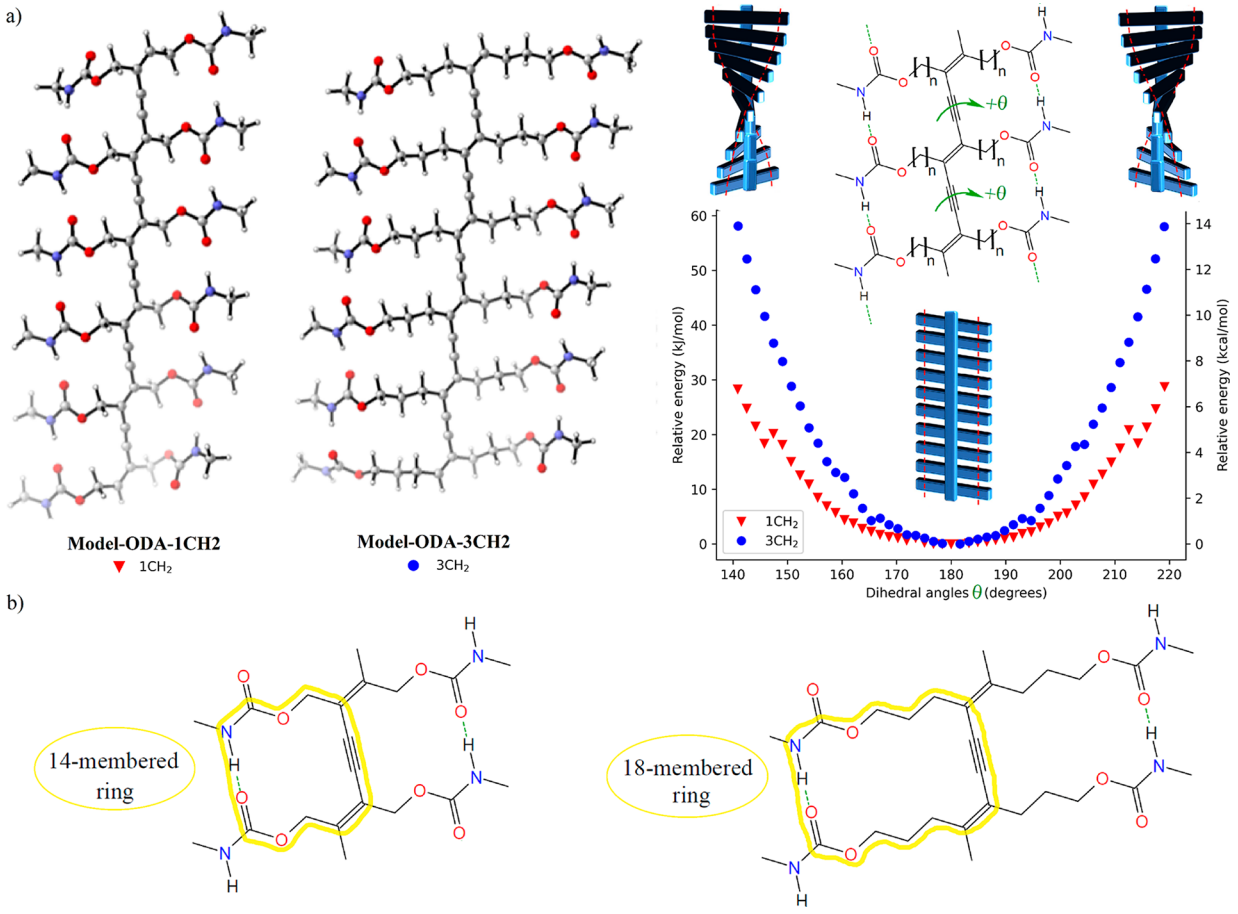

Figure 8. (a) GFN2-xTB (gas phase) energy values for the torsional energy profiles of simplified ODA models with symmetrical carbamate side chains. (b) Illustration of the 14- or 18-membered ring formed depending on the spacer length.

model of 6 hexamers achieves 97% of the maximal interaction energy and appears to be an adequate model of the infinite supramolecular stacking. The same analysis for the noncovalent interactions in **FAM-PDA-3CH2** results in an extrapolated interaction energy of −198.5 kcal/mol, only 0.1 kcal/mol greater than the central HB of the eight hexamers model ($k = 4$, $m = 8$).

Finally, since the PDA chains of (**FAM-PDA-1CH2**) are interlocked by skewed directional and cooperatives HBs to form 2D nanosheets, it is conceivable that these kinds of material could eventually, following a tear, reassemble through the HBs, like a zipper, leading potentially to a new type of healable 2D conjugated polymer.[79]

COMPUTATIONAL STUDIES (PLANAR CONFORMATION: A LOCAL MINIMUM OF POTENTIAL ENERGY?)

To evaluate the ability of PDA chains to form planar or helical conformations with intramolecular HBs, we evaluated the torsional potential of the conjugated PDA backbone. Based on a similar procedure we used in our recent paper on PClDA,[27] we performed dihedral scans with the semiempirical tight-binding GFN2-xTB method (gas phase) on simplified oligodiacetylene (ODA) models (**Model-ODA-1CH2** and **Model-ODA-3CH2**, Figure 8a). The purpose of these calculations was to verify if the helical conformation is preferred when the HBs are close to the backbone (i.e., for **FAM-PDA-1CH2**). In such a case, it could be another factor that supports the preference for **FAM-PDA-1CH2** to not polymerize in the direction parallel to HBs. Indeed, if the helix conformation is lower in energy and an energy barrier must be overcome to reach the planar conformation, this could hinder polymerization in that direction. However, our results show that in both cases, the planar conformation with intramolecular HBs is a local minimum of potential energy, with deviations resulting in a roughly quadratic increase in energy. However, it is easier to access the helices with $n = 1$ than with $n = 3$. Indeed, the torsional energy profiles show that to form a helix with a 30° deviation from planarity, 29−33 kJ/mol is required for $n = 3$, while only 15−18 kJ/mol is required for $n = 1$ (Figure 8a). Based on the Boltzmann distribution, 99% of the population at 298 K is expected to deviate up to 27° from the minimum for $n = 1$, but only 19° for $n = 3$. A possible explanation for this observation is that the formation of HBs close to the conjugated backbone in the planar conformation ($\theta = 180°$) is more difficult to achieve for $n = 1$ than for $n = 3$, as it is more difficult to align the carbamate HBs in a ring consisting of 14 atoms (when $n = 1$) rather than in a more flexible 18 atoms ring (when $n = 3$) (Figure 8b). The energy gap between the planar and helical conformation for $n = 1$ is thus reduced. These computational results highlight the influence of the spacer's length on the polymer's flexibility and may impact the design of PDA materials. Indeed, short spacer length ($n = 1$) may potentially increase the ability to induce planar−nonplanar conformation transitions of the conjugated backbone, which is related to the optoelectronic properties of the PDA chain (e.g., color changes).

https://doi.org/10.1021/acs.cgd.2c00307
Cryst. Growth Des. 2022, 22, 2812−2823

CONCLUSION

We have reported the synthesis and single crystal structure of a novel furfurylamine biobased diacetylene (**FAM-DA**) monomer having three methylene units as a spacer between the carbamate functionality and the DA reactive group. The influence of the spacer length is present, since, with one methylene, the direction of solid-state polymerization is skewed with respect to HB orientation, and with three methylenes, the direction is parallel to it. Our results suggest that, when a choice arises, the polymerization occurs in the direction in which the repeat distance parameter d for polymerization of DA is within the range recommended by Laugher (d = 4.7 to 5.1 Å), even if the other direction have better parameters r and θ. To the best of our knowledge, this is the first clear single crystal structure demonstration on the influence of the spacer length on the direction of polymerization of DA relative to the HB network. Ordering polymers in different packing modes is a challenging task.[80] This study shows that modification of short spacer length allows different alignment of DAs and different packed forms of PDAs, resulting in a new method to tune the properties of polymers. Indeed, we have presented here the ability to obtain different orientations of conjugated polymers through subtle structural changes to the starting diyne derivative. Programming the orientation of π-conjugated polymers is a key facet in the development of organic optoelectronics, since orientation of the polymer chains has a strong influence on the final properties of the material.[81,82] Moreover, computational studies on model oligodiacetylenes built from the crystallographic data of the final PDAs reveal that

- **FAM-PDA-1CH2** forms a 2D nanosheet with a cooperative effect of the interchain HB network. This arrangement with such a strong structure stabilization could potentially be used to design healable 2D conjugated polymer, similar to a previously reported study on self-healable 2D supramolecular PDA material.[79]
- Both PDA chains with intramolecular HBs present a local minimum of potential energy for the planar conformation. However, for **FAM-PDA-1CH2**, the helical conformations are more easily accessible. This preliminary result suggests that short spacer length (n = 1) can potentially increase the ability to make conformational transitions and indirectly affect the design of novel PDA material with specific optoelectronic properties.

Finally, this work on lignocellulosic furfuryl biobased PDA is a new example in the family of furan-containing polymers that have been reviewed in the literature recently.[83−86] Furfuryl groups can act as sites for post-polymerization modification, extending the range of applications for conjugated biobased polymers.[87]

ASSOCIATED CONTENT

Supporting Information

The Supporting Information is available free of charge at https://pubs.acs.org/doi/10.1021/acs.cgd.2c00307.

Experimental details on the synthesis and characterization of compounds **1** and **FAM-DA-3CH2**; IR, NMR, and Raman spectra; recrystallization and polymerization procedure (**FAM-DA-3CH2** → **FAM-PDA-3CH2**); X-ray crystallographic details; and computational details (PDF)

Accession Codes

CCDC 2151365 and 2151367 contain the supplementary crystallographic data for this paper. These data can be obtained free of charge via www.ccdc.cam.ac.uk/data_request/cif, or by emailing data_request@ccdc.cam.ac.uk, or by contacting The Cambridge Crystallographic Data Centre, 12 Union Road, Cambridge CB2 1EZ, UK; fax: +44 1223 336033.

AUTHOR INFORMATION

Corresponding Author

Pierre Baillargeon − *Département de chimie, Cégep de Sherbrooke, Sherbrooke, Québec J1E 4K1, Canada;* orcid.org/0000-0002-2314-2277; Email: Pierre.Baillargeon@cegepsherbrooke.qc.ca

Authors

Raphaël Robidas − *Département de chimie, Université de Sherbrooke, Sherbrooke, Québec J1K 2R1, Canada*

Olivier Toulgoat − *Département de chimie, Cégep de Sherbrooke, Sherbrooke, Québec J1E 4K1, Canada*

Zacharie Michaud − *Département de chimie, Cégep de Sherbrooke, Sherbrooke, Québec J1E 4K1, Canada;* orcid.org/0000-0002-5410-8397

Claude Y. Legault − *Département de chimie, Université de Sherbrooke, Sherbrooke, Québec J1K 2R1, Canada;* orcid.org/0000-0002-0730-0263

Tarik Rahem − *Département de chimie, Cégep de Sherbrooke, Sherbrooke, Québec J1E 4K1, Canada*

Complete contact information is available at: https://pubs.acs.org/10.1021/acs.cgd.2c00307

Author Contributions

The manuscript was written through contributions of all authors. All authors have given approval to the final version of the manuscript.

Funding

P.B. received funding from Fonds de Recherche du Québec—Nature et Technologies (FRQNT, grant No. 2019-CO-254502 and grant No. 2022-CO-302716). C.Y.L. received funding for computational resources from Calcul Québec and Compute Canada.

Notes

The authors declare no competing financial interest.

ACKNOWLEDGMENTS

We thank the Fonds de Recherche du Québec-Nature et Technologies (FRQNT, grant No. 2019-CO-254502 and grant No. 2022-CO-302716) and the Programme d'aide à la diffusion des résultats de recherche au collégial (PADRRC) for financial support. Computational resources were provided by Calcul Québec and Compute Canada. R. R. is grateful to NSERC for a Canada Graduate Scholarship (CGS M), to FRQNT for a Graduate Scholarship (B1X/B2X), and to Hydro-Québec and the Université de Sherbrooke for a Hydro-Québec Graduate Scholarship.

REFERENCES

(1) Wen, J. T.; Roper, J. M.; Tsutsui, H. Polydiacetylene Supramolecules: Synthesis, Characterization, and Emerging Applications. *Ind. Eng. Chem. Res.* **2018**, *57* (28), 9037−9053.

(2) Hall, A. V.; Musa, O. M.; Steed, J. W. Properties and Applications of Stimuli-Responsive Diacetylenes. *Cryst. Growth Des.* **2021**, *21*, 3614−3638.

(3) Kim, C.; Hong, C.; Lee, K. Structures and Strategies for Enhanced Sensitivity of Polydiacetylene (PDA) Based Biosensor Platforms. *Biosens. Bioelectron.* **2021**, *181*, 113120.
(4) Huang, Q.; Wu, W.; Ai, K.; Liu, J. Highly Sensitive Polydiacetylene Ensembles for Biosensing and Bioimaging. *Frontiers in Chemistry* **2020**, *8*, 565782.
(5) Qian, X.; Städler, B. Recent Developments in Polydiacetylene-Based Sensors. *Chem. Mater.* **2019**, *31* (4), 1196−1222.
(6) Qian, X.; Städler, B. Polydiacetylene-Based Biosensors for the Detection of Viruses and Related Biomolecules. *Adv. Funct. Mater.* **2020**, *30* (49), 2004605.
(7) Mittal, A.; Verma, S.; Natanasabapathi, G.; Kumar, P.; Verma, A. K. Diacetylene-Based Colorimetric Radiation Sensors for the Detection and Measurement of γ Radiation during Blood Irradiation. *ACS Omega* **2021**, *6* (14), 9482−9491.
(8) Weston, M.; Kuchel, R. P.; Ciftci, M.; Boyer, C.; Chandrawati, R. A Polydiacetylene-Based Colorimetric Sensor as an Active Use-by Date Indicator for Milk. *J. Colloid Interface Sci.* **2020**, *572*, 31−38.
(9) Fang, F.; Meng, F.; Luo, L. Recent Advances on Polydiacetylene-Based Smart Materials for Biomedical Applications. *Mater. Chem. Front.* **2020**, *4* (4), 1089−1104.
(10) Kim, J.; Moon, B.-S.; Hwang, E.; Shaban, S.; Lee, W.; Pyun, D.-G.; Lee, D. H.; Kim, D.-H. Solid-State Colorimetric Polydiacetylene Liposome Biosensor Sensitized by Gold Nanoparticles. *Analyst* **2021**, *146* (5), 1682−1688.
(11) Qian, X.; Gargalo, C. L.; Gernaey, K. V.; Städler, B. Distinguishing Commercial Beers Using a Solution-Based Sensor Array Derived from Nanoscale Polydiacetylene Vesicles. *ACS Appl. Nano Mater.* **2020**, *3* (4), 3439−3448.
(12) HAO, Y.-J.; ZHU, G.-M. Advances in Fabrication of Polydiacetylene Vesicles and Their Applications in Medical Detection. *Chin. J. Anal. Chem.* **2020**, *48* (2), 164−173.
(13) Perino, A.; Klymchenko, A.; Morere, A.; Contal, E.; Rameau, A.; Guenet, J. M.; Mély, Y.; Wagner, A. Structure and Behavior of Polydiacetylene-Based Micelles. Macromol. *Chem. Phys.* **2011**, *212*, 111−117.
(14) Mauceri, A.; Giansanti, L.; Capitani, D.; Sobolev, A.; Galantini, L.; Bassetti, M.; Nemi, M. G.; Gradella Villalva, D.; Battista, S.; Mancini, G. Cationic Amphiphiles Bearing a Diacetylenic Function in the Headgroup: Aggregative Properties and Polymerization. *Langmuir* **2020**, *36* (41), 12168−12178.
(15) Kumar, R. A.; Jawale, D. V.; Oheix, E.; Geertsen, V.; Gravel, E.; Doris, E. Tailor-Made Polydiacetylene Micelles for the Catalysis of 1,3-Dipolar Cycloadditions in Water. *Adv. Synth. Catal.* **2020**, *362*, 4425.
(16) Ma, B.; Fan, Y.; Zhang, L.; Kong, X.; Li, Y.; Li, J. Direct Colorimetric Study on the Interaction of Escherichia Coli with Mannose in Polydiacetylene Langmuir−Blodgett Films. *Colloids Surfaces B Biointerfaces* **2003**, *27* (2), 209−213.
(17) Geiger, E.; Hug, P.; Keller, B. A. Chromatic Transitions in Polydiacetylene Langmuir-Blodgett Films Due to Molecular Recognition at the Film Surface Studied by Spectroscopic Methods and Surface Analysis. *Macromol. Chem. Phys.* **2002**, *203* (17), 2422−2431.
(18) Wen, J. T.; Bohorquez, K.; Tsutsui, H. Polydiacetylene-Coated Polyvinylidene Fluoride Strip Aptasensor for Colorimetric Detection of Zinc(II). *Sensors Actuators B Chem.* **2016**, *232*, 313−317.
(19) Yu, X.; Zhang, H.; Gao, Y.; Hu, J.; Li, M.-H. Fabrication of Chiral Polydiacetylene Nanotubes via Supramolecular Gelation of a Triterpenoid-Derived Amphiphile. *Mater. Adv.* **2021**, *2*, 3014.
(20) Jang, D.; Pramanik, S. K.; Das, A.; Baek, W.; Heo, J.-M.; Ro, H.-J.; Jun, S.; Park, B. J.; Kim, J.-M. Photoinduced Reversible Bending and Guest Molecule Release of Azobenzene-Containing Polydiacetylene Nanotubes. *Sci. Rep.* **2019**, *9* (1), 15982.
(21) Krishnan, B. P.; Mukherjee, S.; Aneesh, P. M.; Namboothiry, M. A. G.; Sureshan, K. M. Semiconducting Fabrics by In Situ Topochemical Synthesis of Polydiacetylene: A New Dimension to the Use of Organogels. *Angew. Chemie Int. Ed.* **2016**, *55* (7), 2345−2349.
(22) Song, W.; Li, Y.; Geng, L.; Feng, G.; Ren, J.; Yu, X. Polydiacetylene-Based Gels for Solvent Discrimination and Formation of Au/Ag Nanoparticles with Embedded Photocatalytic Performance. *Mater. Des.* **2021**, *205*, 109744.
(23) Chiba, R.; Onodera, T.; Kasai, H.; Oikawa, H. Solid-State Polymerization Behaviors of Polydiacetylene Nanofibers. *Mol. Cryst. Liq. Cryst.* **2020**, *704* (1), 89−96.
(24) Bhattacharjee, A.; Clark, R.; Gentry-Weeks, C.; Li, Y. V. A Novel Receptor-Free Polydiacetylene Nanofiber Biosensor for Detecting E. Coli via Colorimetric Changes. *Mater. Adv.* **2020**, *1* (9), 3387−3397.
(25) Hall, A. V.; Yufit, D. S.; Apperley, D. C.; Senak, L.; Musa, O. M.; Hood, D. K.; Steed, J. W. The Crystal Engineering of Radiation-Sensitive Diacetylene Cocrystals and Salts. *Chem. Sci.* **2020**, *11* (30), 8025−8035.
(26) Dory, Y. L.; Caron, M.; Duguay, V. O.; Chicoine-Ouellet, L.; Fortin, D.; Baillargeon, P. Preparation and Single Crystal Structure Determination of the First Biobased Furan-Polydiacetylene Using Topochemical Polymerization. *Crystals* **2019**, *9*, 448.
(27) Baillargeon, P.; Robidas, R.; Legault, C. Y.; Rahem, T.; Paré Fouapon, A.; Boivin, S.-M. Rapid Access to Polychlorodiacetylene Single Crystals through H-Bond Templating and Computations on Helical PDA Oligomers. *Cryst. Growth Des.* **2020**, *20*, 5648−5656.
(28) Bae, K.; Heo, J.-M.; Khazi, M. I.; Joung, J. F.; Park, S.; Kim, Y.; Kim, J.-M. Macrocyclic Diacetylene−Terthiophene Cocrystal: Molecular Self-Assembly, Topochemical Polymerization, and Energy Transfer. *Cryst. Growth Des.* **2020**, *20* (1), 434−441.
(29) Xu, W. L.; Smith, M. D.; Krause, J. A.; Greytak, A. B.; Ma, S.; Read, C. M.; Shimizu, L. S. Single Crystal to Single Crystal Polymerization of a Self-Assembled Diacetylene Macrocycle Affords Columnar Polydiacetylenes. *Cryst. Growth Des.* **2014**, *14* (3), 993−1002.
(30) Hu, F.; Bi, X.; Chen, X.; Pan, Q.; Zhao, Y. Single-crystal-to-single-crystal Transformations for the Preparation of Small Molecules, 1D and 2D Polymers Single Crystals. *Chem. Lett.* **2021**, *50* (5), 1015−1029.
(31) Zhu, Y.; Shao, P.; Hu, L.; Sun, C.; Li, J.; Feng, X.; Wang, B. Construction of Interlayer Conjugated Links in 2D Covalent Organic Frameworks via Topological Polymerization. *J. Am. Chem. Soc.* **2021**, *143* (21), 7897−7902.
(32) Hema, K.; Ravi, A.; Raju, C.; Sureshan, K. M. Polymers with Advanced Structural and Supramolecular Features Synthesized through Topochemical Polymerization. *Chem. Sci.* **2021**, *12*, 5361−5380.
(33) Hema, K.; Ravi, A.; Raju, C.; Pathan, J. R.; Rai, R.; Sureshan, K. M. Topochemical Polymerizations for the Solid-State Synthesis of Organic Polymers. *Chem. Soc. Rev.* **2021**, *50* (6), 4062−4099.
(34) Enkelmann, V. Structural Aspects of the Topochemical Polymerization of Diacetylenes. *Adv. Polym. Sci.* **1984**, *63*, 91−136.
(35) Fowler, F. W.; Lauher, J. W. A.; Haley, M. M.; Tykwinski, R.R. Solid State Strategy for the Preparation of Carbon-Rich Polymers. *Carbon-Rich Compounds* **2006**, 198−228.
(36) Dautel, O. J.; Robitzer, M.; Lère-Porte, J. P.; Serein-Spirau, F.; Moreau, J. J. E. Self-Organized Ureido Substituted Diacetylenic Organogel. Photopolymerization of One-Dimensional Supramolecular Assemblies to Give Conjugated Nanofibers. *J. Am. Chem. Soc.* **2006**, *128*, 16213−16223.
(37) Patel, G. N.; Miller, G. G. Structure-Property Relationships of Diacetylenes and Their Polymers. *J. Macromol. Sci. Part B* **1981**, *20*, 111−131.
(38) Sun, X.; Chen, T.; Huang, S.; Li, L.; Peng, H. Chromatic polydiacetylene with novel sensitivity. *Chem. Soc. Rev.* **2010**, *39*, 4244−4257.
(39) Tachibana, H.; Kumai, R.; Hosaka, N.; Tokura, Y. Crystal Structures, Polymerization, and Thermochromic Phase Changes in Urethane-Substituted Diacetylenes Crystals with Varying Alkyl Chain Lengths. *Chem. Mater.* **2001**, *13*, 155−158.
(40) Aoki, K.; Kudo, M.; Tamaoki, N. Novel Odd/Even Effect of Alkylene Chain Length on the Photopolymerizability of Organogelators. *Org. Lett.* **2004**, *6* (22), 4009−4012.
(41) Hoofman, R. J. O. M.; Gelinck, G. H.; Siebbeles, L. D. A.; de Haas, M. P.; Warman, J. M.; Bloor, D. Influence of Backbone Conformation on the Photoconductivity of Polydiacetylene Chains. *Macromolecules* **2000**, *33* (25), 9289−9297.

https://doi.org/10.1021/acs.cgd.2c00307
Cryst. Growth Des. 2022, 22, 2812−2823

(42) Fujita, N.; Sakamoto, Y.; Shirakawa, M.; Ojima, M.; Fujii, A.; Ozaki, M.; Shinkai, S. Polydiacetylene Nanofibers Created in Low-Molecular-Weight Gels by Post Modification: Control of Blue and Red Phases by the Odd−Even Effect in Alkyl Chains. *J. Am. Chem. Soc.* **2007**, *129* (14), 4134−4135.
(43) Kampes, R.; Zechel, S.; Hager, M. D.; Schubert, U. S. Halogen Bonding in Polymer Science: Towards New Smart Materials. *Chem. Sci.* **2021**, *12*, 9275−9286.
(44) Berger, G.; Soubhye, J.; Meyer, F. Halogen Bonding in Polymer Science: From Crystal Engineering to Functional Supramolecular Polymers and Materials. *Polym. Chem.* **2015**, *6* (19), 3559−3580.
(45) Sun, A.; Lauher, J. W.; Goroff, N. S. Preparation of Poly(diiododiacetylene), an Ordered Conjugated Polymer of Carbon and Iodine. *Science* **2006**, *312*, 1030−1034.
(46) Luo, L.; Wilhelm, C.; Sun, A.; Grey, C. P.; Lauher, J. W.; Goroff, N. S. Poly(diiododiacetylene): Preparation, Isolation, and Full Characterization of a Very Simple Poly(diacetylene). *J. Am. Chem. Soc.* **2008**, *130*, 7702−7709.
(47) DeCicco, R. C.; Luo, L.; Goroff, N. S. Exploiting Unsaturated Carbon−Iodine Compounds for the Preparation of Carbon-Rich Materials. *Acc. Chem. Res.* **2019**, *52*, 2080−2089.
(48) Jin, H.; Young, C. N.; Halada, G. P.; Phillips, B. L.; Goroff, N. S. Synthesis of the Stable Ordered Conjugated Polymer Poly-(dibromodiacetylene) from an Explosive Monomer. *Angew. Chem., Int. Ed.* **2015**, *54*, 14690−14695.
(49) Bertault, M.; Canceill, J.; Collet, A.; Toupet, L. Synthesis and Solid-State Polymerization Properties of Symmetrical and Unsymmetrical Diacetylene Derivatives Containing a 'Polymerogenic' Side Group. *J. Chem. Soc. Chem. Commun.* **1988**, *3*, 163−166.
(50) O'Dea, R. M.; Willie, J. A.; Epps, T. H. 100th Anniversary of Macromolecular Science Viewpoint: Polymers from Lignocellulosic Biomass. Current Challenges and Future Opportunities. *ACS Macro Lett.* **2020**, *9* (4), 476−493.
(51) Mariscal, R.; Maireles-Torres, P.; Ojeda, M.; Sádaba, I.; López Granados, M. Furfural: A Renewable and Versatile Platform Molecule for the Synthesis of Chemicals and Fuels. *Energy Environ. Sci.* **2016**, *9* (4), 1144−1189.
(52) Chatterjee, M.; Ishizaka, T.; Kawanami, H. Reductive amination of furfural to furfurylamine using aqueous ammonia solution and molecular hydrogen: an environmentally friendly approach. *Green Chem.* **2016**, *18*, 487−496.
(53) Di, J.-H.; Gong, L.; Yang, D.; He, Y.-C.; Tang, Z.-Y.; Ma, C.-L. Enhanced Conversion of Biomass to Furfurylamine with High Productivity by Tandem Catalysis with Sulfonated Perlite and *ω*-Transaminase Whole-Cell Biocatalyst. *J. Biotechnol.* **2021**, *334*, 26−34.
(54) Park, J.; Heo, J.-M.; Seong, S.; Noh, J.; Kim, J.-M. Self-Assembly Using a Retro Diels-Alder Reaction. *Nat. Commun.* **2021**, *12*, 4207.
(55) Vartak, A.; Goins, C.; de Moura, V. C. N.; Schreidah, C. M.; Landgraf, A. D.; Lin, B.; Du, J.; Jackson, M.; Ronning, D. R.; Sucheck, S. J. Biochemical and Microbiological Evaluation of N-Aryl Urea Derivatives against Mycobacteria and Mycobacterial Hydrolases. *Med.Chem.Comm.* **2019**, *10* (7), 1197−1204.
(56) Rosenthal, M.; Li, L.; Hernandez, J. J.; Zhu, X.; Ivanov, D. A.; Möller, M. A Diacetylene-Containing Wedge-Shaped Compound: Synthesis, Morphology, and Photopolymerization. *Chem. − A Eur. J.* **2013**, *19* (13), 4300−4307.
(57) Qi, J.; Kim, Y.; Takahashi, K.; Aoki, K.; Hisaki, I.; Nakamura, T.; Tamaoki, N. A Series of Bisamide-Substituted Diacetylenes Exhibiting a Terminal Alkyl Odd/Even Parity Effect on Mechanoactivated Photopolymerization. *Chem. − A Eur. J.* **2021**, *27* (11), 3832−3841.
(58) Martin, I. J.; Shih, K.-C.; Nieh, M.-P.; Kasi, R. M. Templated Supramolecular Structures of Multichromic, Multiresponsive Perylene Diimide-Polydiacetylene Films. *Macromolecules* **2020**, *53* (11), 4501−4510.
(59) Chernyshov, I. Y.; Ananyev, I. V.; Pidko, E. A. Revisiting van Der Waals Radii: From Comprehensive Structural Analysis to Knowledge-Based Classification of Interatomic Contacts. *ChemPhysChem* **2020**, *21* (5), 370−376.
(60) Menzel, H.; Horstmann, S.; Mowery, M. D.; Cai, M.; Evans, C. E. Diacetylene Polymerization in Self-Assembled Monolayers: Influence of the Odd/Even Nature of the Methylene Spacer. *Polymer* **2000**, *41*, 8113−8119.
(61) Pankaew, A.; Traiphol, N.; Traiphol, R. Synthesis of Color-Responsive Polydiacetylene Assemblies and Polydiacetylene/Zinc(II) Ion/Zinc Oxide Nanocomposites in Water, Toluene and Mixed Solvents: Toward Large-Scale Production. *Colloids Surfaces A Physicochem. Eng. Asp.* **2021**, *617*, 126431.
(62) We have ourselves used the range from 4.7 to 5.2 Å for the repeat distance d in our previous publications since we reported the predominant values in the literature. However, we now believe that the range of 4.7 to 5.1 Å makes more sense, because it is related to a symmetrical deviation from the ideal value of 4.9 Å ($d = 4.9 \pm 0.2$ Å).
(63) Patel, G. N.; Khanna, Y. P.; Ivory, D. M.; Sowa, J. M.; Chance, R. R. Polymer Conversions in the *γ*-Ray Polymerization of Urethane-Substituted Diacetylenes. *J. Polym. Sci. Polym. Phys. Ed.* **1979**, *17* (5), 899−903.
(64) Bai, L.; Han, Y.; Sun, C.; An, X.; Wei, C.; Liu, W.; Xu, M.; Sun, L.; Sun, N.; Yu, M.; et al. Unveiling the Effects of Interchain Hydrogen Bonds on Solution Gelation and Mechanical Properties of Diarylfluorene-Based Semiconductor Polymers. *Research* **2020**, *2020*, 1−15.
(65) Song, P. A.; Wang, H. High-Performance Polymeric Materials through Hydrogen-Bond Cross-Linking. *Adv. Mater.* **2020**, *32*, 1901244.
(66) Kríz, J.; Dybal, J.; Brus, J. Cooperative Hydrogen Bonds of Macromolecules. 2. Two-Dimensional Cooperativity in the Binding of Poly(4-Vinylpyridine) to Poly(4-Vinylphenol). *J. Phys. Chem. B* **2006**, *110*, 18338−18346.
(67) Xiao, T.; Zhou, L.; Sun, X.-Q.; Huang, F.; Lin, C.; Wang, L. Supramolecular Polymers Fabricated by Orthogonal Self-Assembly Based on Multiple Hydrogen Bonding and Macrocyclic Host-Guest Interactions. *Chin. Chem. Lett.* **2020**, *31* (1), 1−9.
(68) Fu, T.; Li, Z.; Zhang, Z.; Zhang, X.; Wang, F. Supramolecular Cross-Linking and Gelation of Conjugated Polycarbazoles Via Hydrogen Bond Assisted Molecular Tweezer/guest Complexation. *Macromolecules* **2017**, *50* (19), 7517−7525.
(69) Gómez, P.; Georgakopoulos, S.; Más-Montoya, M.; Cerdá, J.; Pérez, J.; Ortí, E.; Aragó, J.; Curiel, D. Improving the Robustness of Organic Semiconductors through Hydrogen Bonding. *ACS Appl. Mater. Interfaces* **2021**, *13*, 8620−8630.
(70) Yu, X.; Li, C.; Gao, C.; Zhang, X.; Zhang, G.; Zhang, D. Incorporation of Hydrogen-Bonding Units into Polymeric Semiconductors Toward Boosting Charge Mobility, Intrinsic Stretchability, and Self-Healing Ability. *Smartmat* **2021**, *2* (3), 347−366.
(71) Mullin, W. J.; Sharber, S. A.; Thomas, S. W. Optimizing the Self-Assembly of Conjugated Polymers and Small Molecules through Structurally Programmed Non-Covalent Control. *J. Polym. Sci.* **2021**, *59* (59), 1643−1663.
(72) Zhu, C.; Mu, A. U.; Wang, C.; Ji, X.; Fang, L. Synthesis and Solution Processing of a Rigid Polymer Enabled by Active Manipulation of Intramolecular Hydrogen Bonds. *ACS Macro Lett.* **2018**, *7* (7), 801−806.
(73) Zhang, L.; Ruesch, M.; Zhang, X.; Bai, Z.; Liu, L. Tuning Thermal Conductivity of Crystalline Polymer Nanofibers by Interchain Hydrogen Bonding. *RSC Adv.* **2015**, *5* (107), 87981−87986.
(74) Song, Z.; Fu, H.; Wang, R.; Pacheco, L. A.; Wang, X.; Lin, Y.; Cheng, J. Secondary Structures in Synthetic Polypeptides from N-Carboxyanhydrides: Design, Modulation, Association, and Material Applications. *Chem. Soc. Rev.* **2018**, *47* (19), 7401−7425.
(75) Rossmeisl, J.; Nørskov, J. K.; Jacobsen, K. W. Elastic Effects behind Cooperative Bonding in *β*-Sheets. *J. Am. Chem. Soc.* **2004**, *126* (40), 13140−13143.
(76) Marafon, G.; Motta, M. A.; Toniolo, C.; Moretto, A. From self-assembled peptide-ynes to peptide polyacetylenes and polydiacetylenes. *Peptide Science* **2018**, *110*, e24036.
(77) Kobko, N.; Dannenberg, J. J. Cooperativity in Amide Hydrogen Bonding Chains. Relation between Energy, Position, and H-Bond

https://doi.org/10.1021/acs.cgd.2c00307
Cryst. Growth Des. 2022, 22, 2812−2823

Chain Length in Peptide and Protein Folding Models. *J. Phys. Chem. A* **2003**, *107*, 10389−10395.
(78) Kobayashi, Y.; Saigo, K. Periodic Ab Initio Approach for the Cooperative Effect of CH/π Interaction in Crystals: Relative Energy of CH/π and Hydrogen-Bonding Interactions. *J. Am. Chem. Soc.* **2005**, *127* (43), 15054−15060.
(79) Li, M.; Song, M.; Wu, G.; Tang, Z.; Sun, Y.; He, Y.; Li, J.; Li, L.; Gu, H.; Liu, X.; Ma, C.; Peng, Z.; Ai, Z.; Lewis, D. J. A Free-Standing and Self-Healable 2D Supramolecular Material Based on Hydrogen Bonding: A Nanowire Array with Sub-2-Nm Resolution. *Small* **2017**, *13* (21), 1604077.
(80) Rai, R.; Sureshan, K. M. Topochemical Synthesis of a Heterochiral Peptide Polymer in Different Polymorphic Forms from Crystals and Aerogels. *Angew. Chem., Int. Ed.* **2022**, *61*, e202111623.
(81) Hicks, G. E. J.; Li, S.; Obhi, N. K.; Jarrett-Wilkins, C. N.; Seferos, D. S. Programmable Assembly of π-Conjugated Polymers. *Adv. Mater.* **2021**, *33*, 2006287.
(82) Vohra, V.; Anzai, T. Molecular Orientation of Conjugated Polymer Chains in Nanostructures and Thin Films: Review of Processes and Application to Optoelectronics. *J. Nanomater.* **2017**, *2017*, 3624750.
(83) Gandini, A.; M. Lacerda, T. Furan Polymers: State of the Art and Perspectives. *Macromol. Mater. Eng.* **2022**, 2100902.
(84) Cao, H.; Rupar, P. A. Recent Advances in Conjugated Furans. *Chem. − A Eur. J.* **2017**, *23* (59), 14670−14675.
(85) Zheng, B.; Huo, L. Recent Advances of Furan and Its Derivatives Based Semiconductor Materials for Organic Photovoltaics. *Small Methods* **2021**, *5* (9), 2100493.
(86) Gevrek, T. N.; Sanyal, A. Furan-Containing Polymeric Materials: Harnessing the Diels-Alder Chemistry for Biomedical Applications. *Eur. Polym. J.* **2021**, *153*, 110514.
(87) Farmer, T. J.; Comerford, J. W.; Pellis, A.; Robert, T. Post-Polymerization Modification of Bio-Based Polymers: Maximizing the High Functionality of Polymers Derived from Biomass. *Polym. Int.* **2018**, *67* (7), 775−789.

https://doi.org/10.1021/acs.cgd.2c00307
Cryst. Growth Des. 2022, 22, 2812−2823